



Group project for the course of
Mechanical Design for Mechatronics

Prof.: Rustighi Emiliano

Technical report

**Design of the Structure of an Automated Machine
for Agricultural Purposes**

Bontempelli Elia
Rizzardi Alessandro

Dalle Vedove Matteo
Zambotti Beatrice

August 28, 2022

Contents

1	Product design specification	1
1.1	Requirements & specifications	2
1.2	Goal of our project	2
2	Concept generation	2
2.1	Decision matrix	5
2.2	Material selection	7
3	Preliminary design	8
4	Design process and verifications	11
4.1	Static verification	12
4.2	Fatigue verification	14
4.3	Threaded joints verification	14
4.4	Design and static verification of rack and gear	21
5	Conclusions	23
A	Appendix	24
A.1	Materials	24
A.2	Bill of Materials	25
B	Technical drawings	26
B.1	Gear and rack design	26
B.2	Final CAD	29
B.3	Connection assembly details	31
C	Bibliography and references	37

1 Product design specification

The goal of our project is to create our implementation of the *CyberOrto* [[cyberorto](#)] made by *Mindshub*, a non-lucrative association based in Ala (Trentino). The goal of this robot is to automatically handle an amateur vegetable garden by performing this 3 principle actions:

- i) planting the seeds of the desired plant in a location decided by the user using a web interface;
- ii) constantly provide water to the vegetable;
- iii) extirpate undesired plants.

By talking with the association that worked (and is still improving) on the product we acknowledged the following requirements (mainly related to the functionality of the product) that the machine has to satisfy:

- i) the arm appendix must suits an interface that allows to have an interchangeable set of tools (like the one use to plow the terrain);
- ii) the arm appendix should accommodate a small pipe in order to irrigate the vegetables; in particular this has to be connected to an external reservoir (with no dimension specified if it's position is fixed) or by using an internal reservoir on the moving structure of at least $4l$ (that can periodically be refilled) if it's not possible to directly attach the arm to the main reservoir;
- iii) the minimum accepted working area of the robot is a rectangle of dimension $4m \times 3m$; the robot should be design keeping in mind the possibility to increase the working area by expanding it over one edge (for example having the possibility to work on a $8m \times 3m$ terrain);
- iv) the structure can house the electronic control unit of the robot that's remotely connected to the server using wireless connection and by doing so should accommodate a battery that allows the robot to work for at least $4h$. The power consumption of the structure should be minimized if possible (at the actual state the prototype consumes $40W$ and has a battery of $240Wh$ weighting $6.3kg$);
- v) regarding the accuracy of the movement of the system the allowed backlash on the working point should always be less than $1cm$ with the control technique implemented and the goal is to have maximum $5mm$ of deviation from the nominal value;
- vi) the structure should be mainly composed of standard components and should be as cheap as possible in order to make it affordable for everyone.

Loads and operating conditions The structure should be able to perform all its operation while being safe and fully functional. For the design and the verification of the structure the loads related to wind can be neglected due to the presence of an anemometer that's mounted on the robot that's ensuring that the robot works only on a sufficiently safe environment.

The heavier operation performed by the robot is the extirpation that's done by plowing the soil with a rotating disk attached to a motor that uses three nails to move the terrain in the nearby of the target zone. In the current state the mounted motor that performs this operation exerts a torque $T_{\text{plower}} = 0.8N \cdot m$ and it's consider as the value that will be used for our dimensioning and verification phases.

1.1 Requirements & specifications

With this promise being said, it's possible to express the main requirements, associated to the aim dictated by our customer and our design rules, and the specifications of the designed machine. All this information, collected in table 1, has to be considered in each step of the design phase in order to develop the mechanical solution.

While developing the project other factors should be kept in mind:

- the possibility to pack all the necessary components in a *small* transportation box (the box shouldn't present and edge greater than $2m$, maximum sum of all the edges less then $3m$) in order to avoid shipping issues;
- the kit should be feasible to all private enthusiast that enjoy *do-it-yourself* projects and this has to kept in mind; the final assembly should be made possible by common mounting tools (such screwdrivers, Allen keys...) that can be easily purchased and used by the customer; for the same reason welding finishes are not recommended.

1.2 Goal of our project

Designing the whole machine is out of our scopes as it is very complex and requires knowledge that we still miss, so we decided to focus our work in the design of the main structure of the robot putting effort in the structural verification as the goal of the course.

2 Concept generation

With all the premise that lead the development of the project, the first thing that has to be done is generate the concept that can later be compared to choose the best design solution that can become a concrete realization of the ideas.

Kinematic configurations The first key operation that the robot has to perform is reaching a desired point on the working space and so, in planar kinematics, the machine should present two degrees of freedom that allow to reach all the possible positions; this can be done considering 3 main joint configuration that allows to perform such operations:

- double prismatic joints (figure 1.a) where two perpendicular linear guides can be used to move on the plane;
- prismatic and revolute joint (figure 1.b) where the arm that's free to rotate it's mounted on top of a linear guide. This kind of kinematic chain is currently used by the MindsHub concept;

Table 1: full list of requirements and specifications for the CyberOrto project.

1) Geometry:		
1.1) dimension of the terrain to cultivate	at least $4m \times 3m$, extendible if possible	
1.2) vertical clearance from the ground of the robot while moving	$\geq 50cm$	
2) Kinematic:		
2.1) time travel between further points in the field	$\leq 10s$	
2.2) accuracy of the working appendix respect to nominal value	max $\pm 1cm$, target $\pm 5mm$	
3) Energy:		
3.1) low energy consumption	max $40W$, target $20W$	
3.2) in-device battery with docking station	battery $\geq 240Wh$ or 4+ hour of work	
4) Functionalities:		
4.1a) provide direct water access to irrigate the soil		
4.1b) or provide a reservoir that can be automatically refilled on a docking station	$\geq 4l$	
4.2) standard mount on the appendix arm that can fit multiple working tools		
4.3) plowing the terrain	$T_{\text{plower,max}} = 0.8N \cdot m$	
4.4) provide a pneumatic circuit used for the appendix that plants seeds		
5) Materials:		
5.1) components standardization	very high	
5.2) materials should be weather proof (oxidation free)		
6) Terms of use:		
6.1) easy to assemble		
6.2) fatigue resistance	max 2 persons required infinite life-cycles if possible, min 10^6	
6.3) insensible to environmental conditions (weather and dirt)		
7) Loading conditions:		
7.1) wind and environmental actions can be neglected with robot in action		
8) Costs:	$\leq \text{€}2\,000$	

- double revolute joints (figure 1.c), typical configuration of a robot arm, that constraint the framing point to be fixed.

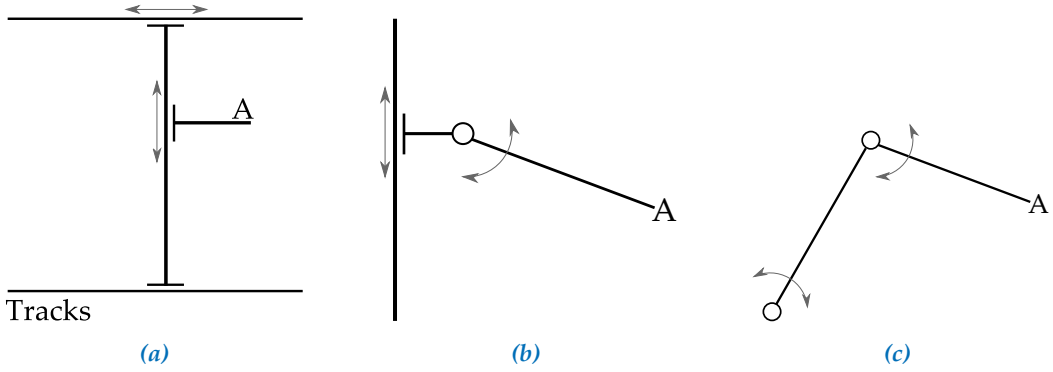


Figure 1: main kinematics coupling that allows to univocally determine the position of a point A in a plane: (a) double prismatic joints, (b) prismatic and revolute joint, (c) double revolute joints.

By a first analysis the third configuration (double revolute joint) isn't feasible for the project due to the fact that the system presents a fixed pivot point respect to the frame and to work more area it's mandatory to increase the length of the edges (and this is an issue for the *extendibility* of the machine).

Concept #1 The first concept (figure 2) is realised with a double prismatic joint. In particular point A and A' lies on parallel tracks placed on the ground that can be extended in order to increase the cultivated area. The working arm can move along an elevated beam connecting the track (point B) and can move vertically to cultivate point P.

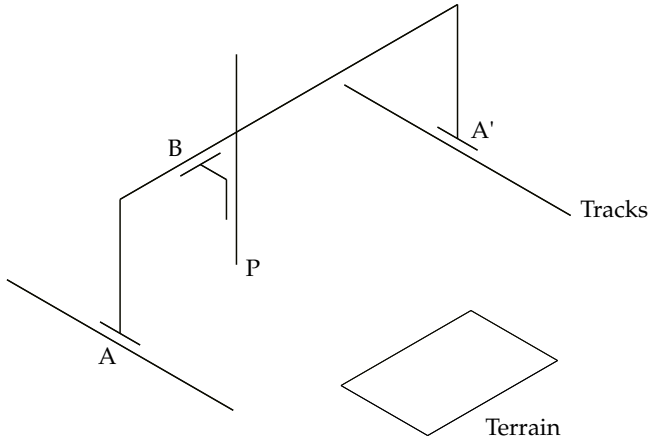


Figure 2: concept #1 realised with double prismatic joint.

This structure present a frame for the arm that's stable while operating due to its arch structure; possible problem to this implementation is that long elevated beam (subjected to the loads of the arms and its mass) can deflect and fail statically. Also, if possible, rotoidal coupling should be used (and for this we can refer to concept #2).

Concept #2 The second concept (figure 3) is similar to the first one but one prismatic joint is replaced with a revolute connection put in the middle of the elevated beam. The length of the edge BP from a top view must be equal to half the length of the supporting bar in order to reach all points in the rectangular space.

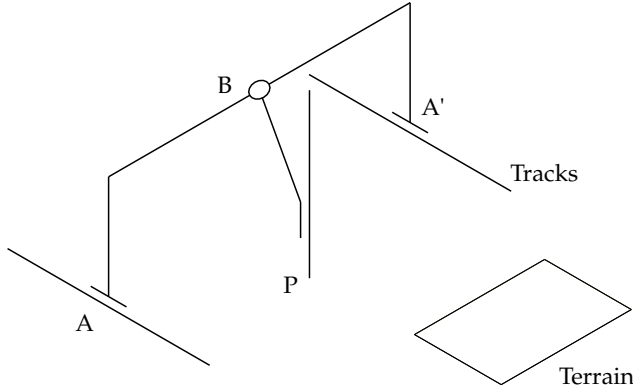


Figure 3: concept #2 realised with a combination of both prismatic and revolute joint.

This structure also presents the pro of concept #1 of having a stable frame structure for the operating arm due to its arch conformation and, as addition, uses a revolute joint to control the second degree of freedom of the arm. However this implementation increases the mechanical load on the elevated beam (increasing the torsion due to the higher arm of the actions on the tool tip respect to the elevated bar).

Concept #3 The third concept (figure 4) is similar to #2 but instead of using two parallel tracks, the prismatic joint uses only one of them.

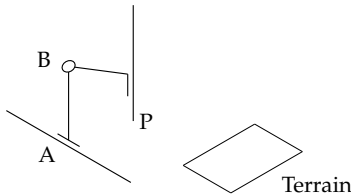


Figure 4: concept #3 realised with a combination of both prismatic and revolute joint.

This implementation avoid the problem of high deflection of concepts #1 and #2 by removing the long elevated framing beam, but also increases the reactional momentum that the prismatic joint A should bear in order to maintain stable the system.

2.1 Decision matrix

With a brief overview of the 3 main concept generated, the unbiased choice can be performed by constructing and evaluating the decision matrix (table 2). The main objective evaluated are:

- costs: based on the estimated material cost considering quantity and types of parts that can be used for the implementation;
- reliability: expected mechanical resistance of the structure subjected to nominal loads as well as unexpected external loads (such environment of customer that interact with the structure);

Table 2: decision matrix.

Objective	Weight	Parameter	Concept #1			Concept #2			Concept #3		
			Mag	Score	Value	Mag	Score	Value	Mag	Score	Value
Material costs	0.2	relative €	medium	7	1.4	high	5	1	low	9	1.8
Reliability	0.3	experience	good	8	2.4	okay	6	1.8	poor-fair	3	0.9
Lifetime	0.15	experience	great	10	1.5	good	8	1.2	fair	4	0.6
Adaptability	0.2	experience	good	8	1.6	okay-good	7	1.4	fair	4	0.8
Team experience	0.15	experience	good	8	1.2	great	10	1.5	fair	4	0.6
Overall score:			8.1			6.9			4.7		

Qualitative score assignments: poor = 2, fair = 4, okay = 6, good = 8, great = 10.

- lifetime: expected lifetime of the product based on fatigue considerations;
- adaptability: criteria that evaluates how easy is to modify geometrical parameters to meet specific custom requirement of the final customer based on asperity and tolerances of the terrain to cultivate;
- team experience: based on the overall design feasibility made by the team.

With the decision matrix completed the chosen concept is the first on which the motion is performed only by prismatic joints.

2.2 Material selection

The main structural components are beams that, for client requirements, should be standard and so for this reason T slot extruded aluminium profiles (figure 5) are chosen after the following considerations:

- better volume-to-price ratio and lower density (respect to inox steels), so reducing costs associated to the spare parts and shipping;
- availability in the market: there are a lot of vendors that provide profiles with various geometrical dimensions, different aluminium alloy and surface finishes. This spare parts can be easily accessed by every private costumer;
- for T slot extruded profiles lots of auxiliary components (such supporting brackets, fasteners, hinges...) are provided from the same profiles manufacturers, reducing the need of custom made part and so decreasing the overall costs.

This elements can be also purchased with an anodized finish that allows to improve the corrosion resistance, increasing so the expected life time of the product in uncontrolled outdoor environment.

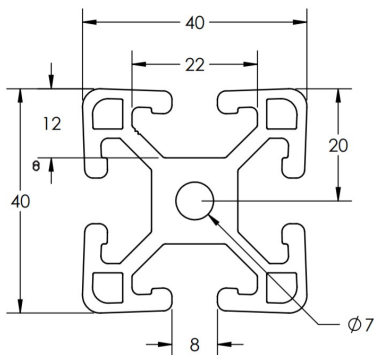


Figure 5: technical drawing of a T-slot profile's cross-section. The particular sketch represent the model TS40-40LM by Tslots [tslot-ds].

Mechanical properties For the design part the following mechanical properties are considered: ultimate tensile strength $\sigma_{uts} = 260\text{MPa}$, yielding strength $\sigma_{ys} = 240\text{MPa}$, Young's module $E = 70\text{GPa}$, Poisson's ratio $\nu = 0.32$; these values are chosen according to table A.1.1 (page 24) as they represent a lower bound (implying higher safety in calculations) for the aluminium material used for the T-Slot sections.

3 Preliminary design

Based on the selected concept the simplest body diagram has been created in order to start the dimensioning of the main elements of the structure. Considering the possible practical implementation of the system, the symbolic representation of the moving frame has been made (figure 6).

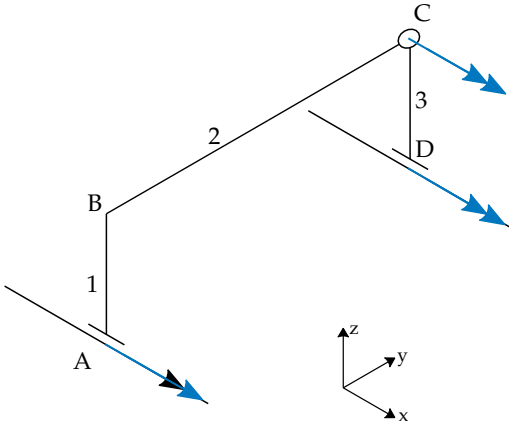
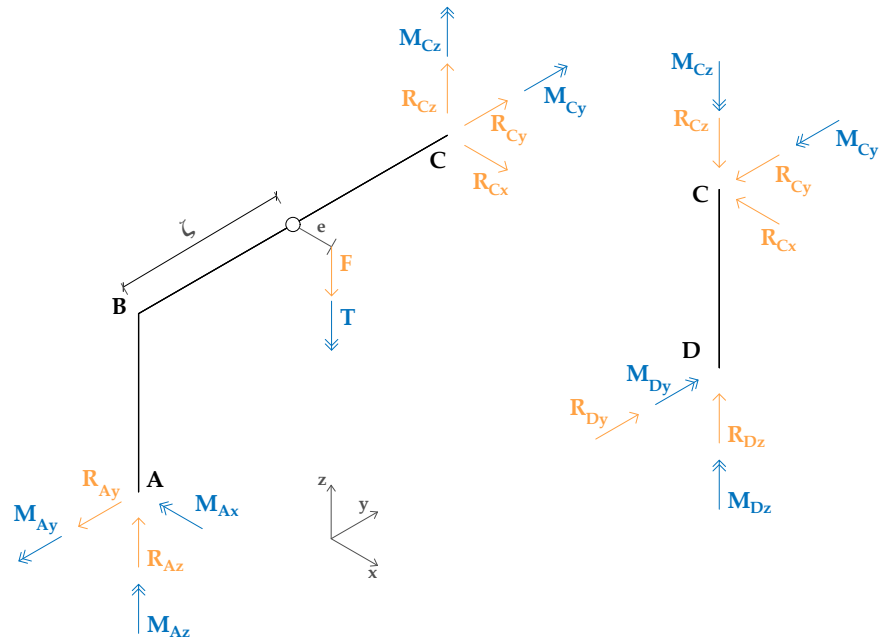


Figure 6: schematic representation of the moving frame supporting the arm; blue arrows are describes the rotational degree of freedom left by the joints.

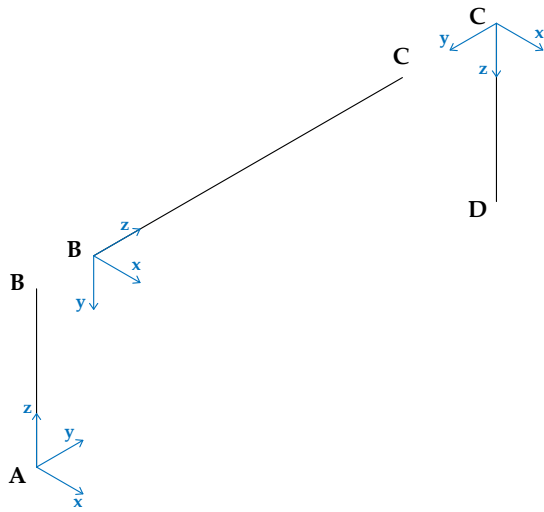
The design involves a main elevated track (body 2) supported by two vertical supporting beams (bodies 1 and 3); the connection between body 1 and 2 is constituted by a full joint in point B constraining all 6 degrees of freedom while the connection of the track with the other support is done by a hinge that leaves free the rotation over the global x axis. The two vertical supports can slide on two parallel tracks and the associated prismatic joints constraints respectively 5 and 4 degrees of freedom in A and D , leaving the system free to slide along the x global axis; the choice of leaving also D in as free to rotate aims at reducing redundant constraints, with the aim of reducing hyperstatic variables with a design that accommodates misalignments in the position of the two parallel tracks placed at ground.

As simplification on both the geometry and the load we consider:

- on the elevated track the loads transferred by the working appendix are modelled as a pure vertical force F (mainly related to the approximate weight of the turret that contains all equipment) and a torque T that model's the one due to the plow; the eccentricities of both forces are in this case neglected and the application of application of both actions is placed at a distance ζ referred to the local coordinate z of the elevated track, figure 7(b);
- the vertical supports are equally dimensioned and present a characteristic height $H = 700mm$; the elevated track connecting them has length $L = 3000mm$ as dictated by the customer requirements;
- figure 7(a) shows the free body diagram of the structure and thus the set of external actions and reactions applied; figure 7(b) reports instead the reference frames with respective origin with respect to which internal loads are calculated.



(a)



(b)

Figure 7: free body diagram (a) and reference frames (b) used for the description of the internal loads of the beam. In (a) the structure has been disassembled at the pivot point C in order to describe the reaction forces transmitted.

The full joint in B has not been described (as the connection preserves the continuity of the actions transmitted by the body), however the final design will imply the connection of two separate beams by means of a gusset.

After having written the Newton-Euler equations of the two bodies making the whole structure, we observe that only 11 out of 14 reactions forces are independent; chosen the hyperstatic variables $X_1 = M_{Az}$, $X_2 = M_{Dy}$, $X_3 = M_{Ax}$ to reduce the problem to an isostatic one, the parametric definitions of the reaction forces is

$$R_{Az} = \frac{F(L - \zeta) - X_3}{L} \quad R_{Cz} = R_{Dz} = \frac{F\zeta + X_3}{L}$$

$$M_{Ay} = M_{Cy} = X_2 \quad M_{Cz} = M_{Dz} = T - X_1$$

Non mentioned actions are identically zero. To solve the hyper-static problem the Castigliano's theorem has been used, computing the elastic energy U_e of the structure neglecting shear loads:

$$U_e = \sum_{i=1}^3 \int_0^{l_i} \left(\frac{N_i^2}{2EA_i} + \frac{M_{x,i}^2}{2EI_{xx,i}} + \frac{M_{y,i}^2}{2EI_{yy,i}} + \frac{M_{z,i}^2}{2GJ_{t,i}} \right) dz$$

Assuming the generalized displacement related to the hyper-static variables is zero, solving the equations $\partial U_e / \partial X_1 = 0$ and $\partial U_e / \partial X_2$, the solution that we achieve is still depending on the geometrical parameters of the sections that are still unknown. To simplify the calculations, assuming that A_1 gives

$$X_1 = T \quad X_2 = 0 \quad X_3 = F \frac{L - 2\zeta}{2}$$

In this preliminary design phase in order to over-estimate the loads the frame should bear a force $F = 200N$ is considered (modelling the weight of about 20kg, related to all the carried equipment on the moving arm including batteries and filled water tank) and the nominal value of the torque $T = 0.8N \cdot m$ as in the requirements specification.

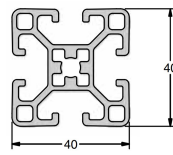
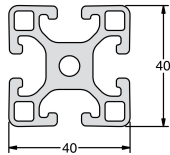
Choice of the standard beams With the preliminary design model described, different solutions can be found looking from various vendors present in the market. In particular for the project main reference has been made to the Parker IPS catalogue [[parker-ds](#)] due to the high availability of accessories components, however similar product can be found by other vendors (as group we also evaluated 8020 [[8020-ds](#)] and Tslots by Bonnel Aluminum [[tslot-ds](#)]).

Data-sheets presents information about the section area A and second moments of area I_{xx} , I_{yy} respect the primary axes, however no information is given for the torsional rigidity J_t and so the related component is in the calculation neglected.

After an iterative process, table 3 shows the sections drawing and associated geometric properties of the chosen components for both elevated track and supporting beams. This choice determines a safety factor $\phi = 3.8$ for the whole structure that's a safe value for us; it is true that we neglected both shear and torque loads, and in practical applications other external and unexpected actions might act on the frame, however it is also true that the geometric simplification A_1 in the solution of the hyperstatic problem heavily reduced the ability of the system to bear load (as we will see in the static verification).

Table 3: selected beams section chosen from the Parker IPS catalogue [parker-ds] and related main properties (area, moments of inertia and weight per unit length).

Usage	Area $A [cm^2]$	Moments of inertia $I_{xx} [cm^4]$	$I_{yy} [cm^4]$	Weight $\rho [kg/m]$	Product code
track	6.65	9.46	9.46	1.72	10-040
supports	5.20	8.27	8.27	1.41	10-540



Sections for the track beam (on the left) and the supports (right).

As a side note, our design was forced to use the 40mm T-slot series (even if a 30mm profile would have let us achieve similar results with lower weights and costs) as it's the only one that disposes off-the-shelf linear roller system that can be easily mounted and used (choosing other profile series would have ended in custom solution that's undesired by the product design specifications).

4 Design process and verifications

With the data obtained from the preliminary analysis, the design has been carried using the 3D CAD software AutoDesk Inventor Professional with the help of the components library provided by the manufacturer Parker IPS. At this stage what we mainly did was to *give shape* at the chosen concept by using mechanical elements provided by the library only in order to minimize the need of custom-made parts.

For actuating the machine no off-the-shelf solution are available, hence we decided to create our custom rack design (see B.1, page 26): such component is made by a set of smaller bid that can be 3D printed with plastic material; such elements can be joined together by means of standard T-slot components. The rack is mounted on both tracks placed at the ground (motion in the x direction) and the elevated one (motion in the y direction); the gear attached to the motor that's actuating the system is a standard element made out of steel. Proper static verification of the component will be described in the following pages.

Using the theory from the course we performed a static verification of the machine and we verified two critical bolted joints.

4.1 Static verification

With all the geometrical values known, it has been possible to carry out a more detailed analysis. Considering a more complex model of the forces that takes into account also the distributed load due to the gravity and that the force F is applied with an eccentricity $e = 5\text{cm}$, it has been possible to parametrically define the hyperstatic variables as

$$X_1 \simeq (0.63 - 0.16\zeta) N \cdot m \quad X_2 \simeq -8.10 N \cdot m$$

$$X_3 \simeq (-10.54 - 11.07\zeta + 55.53\zeta^2 - 6.17\zeta^3) N \cdot m$$

Evaluating the stress state on the 3 beams making up the structure for values of $\zeta \in [0, L]$, what we obtained is that the most critical section is in the elevated track for $\zeta^* = 1.65\text{m}$ at $z^* = 1.65\text{m}$ where the maximum bending value $M_x^* \simeq 135.64\text{N} \cdot \text{m}$ is achieved (as showed in figure 8). Knowing that $N^* = 0$ and neglecting the shear stress contribution due to both shear $V_y^* \simeq 111\text{N}$ and torque $M_z^* \simeq 1.89\text{N} \cdot \text{m}$, the stress state is

$$\sigma_{zz}(y) = \frac{M_x^*}{I_{xx,track}} y \quad \Rightarrow \quad \sigma_{zz,max} = \sigma_{zz}(2\text{cm}) \simeq 28.68\text{MPa}$$

This leads to a safety factor of $\phi = \sigma_{ys}/\sigma_{zz,max} \simeq 8.37$, meaning that the structure is statically verified. This value is more than twice than the one achieved in the preliminary design phase but is due to the fact that in this case the full analytical solution of the hyperstatic problem has been considered, having determined all geometrical properties of the sections. As a reminder:

- due to the lack of analytical formulas for such complex geometry section, shear components due to torque and shears are neglected and could have influenced the mechanical system;
- we did not consider external forces acting that might act on the global x axis due to the actuation of the machine or accidental load applied by the end user: this can lead to an increase in bending and torques that might make the system fail; a high safety factor ensures us the reliability of the system also in such conditions.

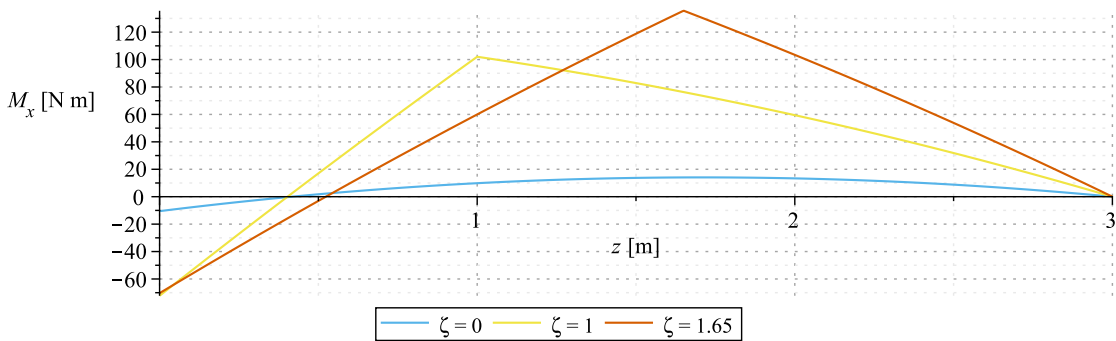


Figure 8: bending moment M_x acting along the elevated track for 3 values of application point of the force; the first case is the minimum-stress condition, while the third one has the maximum bending peak value.

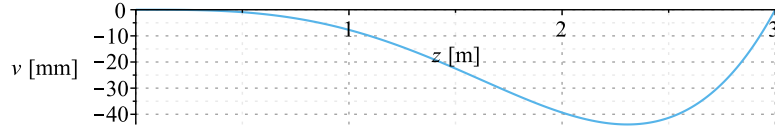


Figure 9: vertical displacement of the turret from the nominal configuration.

Stiffness verification At this point we can also perform a stiffness verification to understand the behaviour of the mechanical system, in particular the displacement with respect to the nominal position of the turret used to perform the operation to the soil. Given the high safety factor and observing that axial load are not that relevant, we can assume the two supports as rigid bodies. At this we consider the radial displacement $v(t)$ from the nominal configuration as related only at the bending action by the law

$$v(z) = -\frac{M_x}{2EI_{xx}}z^2$$

In our study case we have that M_x depends on the point of application of the external force F that's function of ζ , the position of the turret itself (so our point of interest). This allows us to plot the vertical displacement of the turret as function of the position of the turret as in figure 9.

The reported graph contradicts a requirement of our customer as the maximum displacements is bigger than 4cm, exceeding the minimum target displacement value of 1cm. This suggest that the chosen profile 10-040 is not able to withstand all the requirements. In order to avoid this problem two ways can be followed:

- use the mathematical model of the machine in the control system to compensate for such displacement;
- use a different profile with better response at deflection. Looking at the IPS catalogue, a suitable alternative is the 10-080 profile whose section is reported in figure 10. Such beam is characterized by a moment of inertia $I_{xx} = 71.56\text{cm}^4$: neglecting the difference in weight contribution of the bar (whose density is increased to $\rho = 3.18\text{kg/m}$), the maximum displacement is reduced to less then 6mm, fully satisfying the customers requirement.

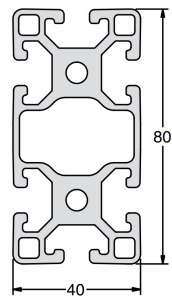


Figure 10: section of the 10-080 T-slot profile by Parker IPS[parker-ds].

In the following (and also in the final CAD) the solution based on the 10-040 profile is reported, however, due to the high *modularity* provided by the T-slot profiles, assembling the machine with the 10-080 component will be practically the same.

4.2 Fatigue verification

Most critical section As already stated, the most critical section is subjected to a maximum stress of $\sigma_{max} \simeq 28.68MPa$. While functioning we expect that the turret performing the operation to the soil periodically moves along the track: having ζ varying over time determines that also the internal loads are fluctuating and this might arise fatigue failure of the machine.

Given the need of a fatigue verification, acknowledged that the minimum bending load at z^* is $M_{x,min} \simeq 14.05N \cdot m$ achieved for $\zeta = 0m$, determining $\sigma_{min} \simeq 2.97MPa$; this further implies that the mean and amplitude stresses for fatigue verification are

$$\sigma_m \simeq 15.82MPa \quad \sigma_a \simeq 12.85MPa$$

According to Soderberg criterion, the equivalent amplitude only stress component evaluates to

$$\sigma_{a,eq} = \frac{\sigma_{ys}\sigma_a}{\sigma_{ys} - \sigma_m} \simeq 13.76MPa$$

In this case the load factor is $C_l = 1$; given an equivalent diameter $d_{eq} = \sqrt{\frac{4}{\pi}A} = 29mm$, the corresponding size factor is $C_d = 1.189d_{eq}^{-0.097} \simeq 0.86$; details concerning the surface finish of the T-slot beams are not enough to fully determine the surface coefficient C_s that's assumed in this case to be 0.8 as safety value. Considering an endurance limit of the 6061-T5 aluminium alloy of $\sigma_{lim} = 100MPa$ [aluminium-endurance], this means that the safety factor against fatigue failure is

$$\phi_{fatigue} = C_s C_d C_l \frac{\sigma_{lim}}{\sigma_{a,eq}} \simeq 4.98$$

4.3 Threaded joints verification

Preliminary design

Given the customer's requirements, the threaded fasteners used for the threaded joints in the whole robot are chosen to be standard screws with diameter of $8mm$, compatible with the $40mm$ T-slot profiles.

Considering the threaded joints present on the robot, the maximum thickness of the members is given by the sum between the beam cross section's width, $40mm$, and the machined gussets thickness, $8mm$. Given that two screws must fit, as in section A, the length of the screws is chosen to be equal to $18mm$, according to UNI ISO 888; table 4 reports the main properties of the chosen bolt used for the verification of the connections.

With reference to figure 6, threaded joints are present in sections A, B, C and D. The verifications are carried out with respect to the most critical sections which, according to the load analysis performed previously, are identified as section A and D. Moreover, since the load distribution depends on the position of the point of application of the external load, the most critical condition corresponds to the one in which the load is applied in $\zeta = 1$ for section A and $\zeta = 3$ for section D.

Table 4: selected bolt chosen from the Parker IPS catalogue [parker-ds] and related main properties.

Parameter	symbol	value
diameter	d	8mm
head diameter	d_0	14mm
length	l	18mm
cross-section	A_b	$16\pi mm^2$
tensile cross-section	A_{bt}	$36.6mm^2$
ultimate tensile strength	σ_{uts}	505MPa
product code		24-118-8

Section A

The loads applied on section A are the following:

- axial load $N_A = -251.13N$;
- bending moment $M_{xA} = -12.65N \cdot m$;
- bending moment $M_{yA} = 1.89N \cdot m$;
- torque $M_{zA} = -0.59N \cdot m$.

In correspondence of section A, there are two machined gussets chosen from the Parker IPS catalogue [parker-ds], reported in figure 11. Given the geometry of the component, the threaded joints are positioned on the vertical z and horizontal x global axis. For this reason, two separated analysis are performed.

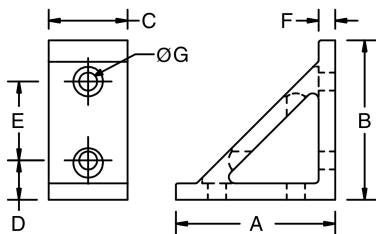


Figure 11: machined gusset, code 10-102, from the IPS catalogue [parker-ds]. In the drawing: $A = 77mm$, $B = 77mm$, $C = 34mm$, $D = 20mm$, $E = 40mm$, $F = 8mm$, $G = 9mm$.

Threaded joints along the x axis The loads acting on section A the x axis are represented in figure 12.

The sliding actions are given by the torque M_{zA} , which produces a shear force on every screw equal to:

$$V_i = \frac{M_{z1}r_i}{\sum_{i=1}^{n_b} r_i^2}$$

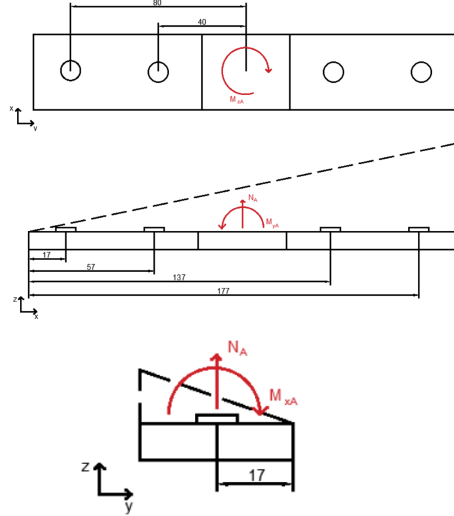


Figure 12: Loads on section A, along the x axis.

where r_i are the distances of every screw from the center of the section, and are equal to $r_1 = 40\text{mm}$, $r_2 = 80\text{mm}$. The shear force is calculated for the most critical screws, distant r_2 , and it is equal to:

$$V_2 = \frac{M_{zA}r_2}{2r_1^2 + 2r_2^2} = -2.97\text{N}$$

The shear and punching resistance verifications can be performed as follow:

- shear resistance verification:

$$|V_2| < \frac{\sigma_{uts}A_b}{\phi}$$

where σ_{uts} corresponds to the screw's ultimate tensile strength, A_b to the bolt cross-section and ϕ is the safety factor which, according to Eurocode3, is equal to $\frac{1.25}{0.58}$. As a consequence, it follows that:

$$\sigma_{uts} > \frac{|V_2|\phi}{A_b} = 0.13\text{MPa}$$

- crushing resistance verification:

$$|V_2| < \frac{\sigma_{uts,m}dt}{\phi}$$

where $\sigma_{uts,m}$ corresponds to the member's ultimate tensile strength, d to the bolt diameter and ϕ is the safety factor which, according to Eurocode3, is equal to 0.5. Finally, t corresponds to the member's thickness, which can be calculated as the sum of the machined gusset thickness, $F = 8\text{mm}$, and the base's thickness, equal to 16mm :

$$\sigma_{uts,m} > \frac{|V_2|\phi}{dt} = 7.73 \cdot 10^{-3}\text{MPa}$$

Separating actions are given by the axial load and the bending moments.

Assuming that the members are rigid it is possible to calculate the effects of the separating actions in both xz and yz planes.

The load caused by the separating action, acting on each bolt can be calculated as:

$$N_i = \frac{M_b h_i}{\sum_{i=1}^{n_b} h_i^2} + \frac{N}{n_b}$$

Considering the xz plane and assuming that the pivot is placed on the edge of the section, the constant h_i will be equal to:

$$\begin{cases} h_1 = 17mm \\ h_2 = 57mm \\ h_3 = 137mm \\ h_4 = 177mm \end{cases}$$

The normal load is calculated for the most critical screw as follow:

$$N_{xz} = \frac{M_{yA} h_4}{h_1^2 + h_2^2 + h_3^2 + h_4^2} + \frac{N_1}{n_b} = -56.53N$$

Since the axial load acting on every bolt is negative, i.e. the bolt are subjected to compression, there are no issues relative to tension and punching resistance. As a consequence, it is not necessary to perform those verifications.

Considering the yz plane and assuming that the pivot is placed on the edge of the section, the constants h_i will be all equal to $h = \frac{C}{2} = 17mm$. The normal load is equal to:

$$N_{yz} = \frac{M_{xA} h}{4h^2} + \frac{N_1}{n_b} = 123.18N$$

The tension resistance and punching verification can be performed as follow:

- tension resistance verification:

$$N_{yz} < \frac{\sigma_{uts} A_{bt}}{\phi}$$

Where σ_{uts} corresponds to the screw's ultimate tensile strength, A_{bt} to the bolt tensile cross-section and ϕ is the safety factor which, according to Eurocode3, is equal to $\frac{1.25}{0.9}$. As a consequence, it follows that:

$$\sigma_{uts} > \frac{N_{yz}\phi}{A_{bt}} = 4.67MPa$$

- punching resistance verification:

$$N_{yz} < \frac{\pi d_0 t \sigma_{uts,m}}{\phi}$$

Where $\sigma_{uts,m}$ corresponds to the member's ultimate tensile strength, d_0 the bolt head diameter and ϕ is the safety factor which, according to Eurocode3, is equal to $\frac{1.25}{0.6}$. Finally, t corresponds to the member's thickness, which can be calculated as the sum of the gusset's thickness, $F = 8mm$, and the base's thickness, equal to $16mm$:

$$\sigma_{uts,m} > \frac{N_{yz}\phi}{\pi d_0 t} = 0.24MPa$$

Threaded joints along the z axis The loads acting on section A the z axis are represented in figure 12.

In this case the sliding actions are given by M_{xA} and N_A which produce a shear force

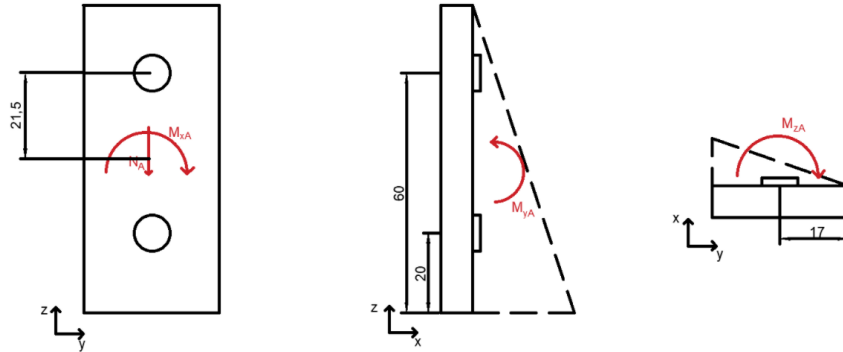


Figure 13: Loads on section A, along the z axis.

on every screw equal to:

$$V_i = \frac{M_{xA}r_i}{\sum_{i=1}^{n_b} r_i^2} + \frac{N_A}{n_b}$$

where r_i are the distances of every screw from the center of the section, and are equal to $r = 21.5\text{mm}$.

$$V = \frac{M_{xA}r}{2r^2} + \frac{N_A}{2} = 140.41\text{N}$$

- shear resistance verification:

$$\sigma_{uts} > \frac{V\phi}{A_b} = 6.20\text{MPa}$$

- crushing resistance verification:

$$\sigma_{uts,m} > \frac{V\phi}{dt} = 0.18\text{MPa}$$

The separating actions, M_{yA} and M_{zA} generates normal load on each and the effects are studies as previously for yz and xy plane.

$$N_i = \frac{M_b h_i}{\sum_{i=1}^{n_b} h_i^2} + \frac{N}{n_b}$$

Considering the yz plane and assuming that the pivot is placed on the edge of the section, the constants h_i will be equal to $h_1 = D = 20\text{mm}$ and $h_2 = D + E = 60\text{mm}$. The normal load is evaluated for the most critical screw and is equal to:

$$N_{xz} = \frac{M_{yA}h_2}{h_1^2 + h_2^2} = 28.40\text{N}$$

- tension resistance verification:

$$\sigma_{uts} > \frac{N_{yz}\phi}{A_{bt}} = 1.08 MPa$$

- punching resistance verification:

$$\sigma_{uts,m} > \frac{N_{yz}\phi}{\pi d_0 t} = 27.46 \cdot 10^{-3} MPa$$

Finally, considering the xy plane, assuming that the pivot is placed on the edge of the section, the constants h_i will be all equal to $h = \frac{C}{2} = 17mm$ the normal load is equal to:

$$N_{xy} = \frac{M_{zA}h}{2h^2} = 17.47N$$

- tension resistance verification:

$$\sigma_{uts} > \frac{N_{xy}\phi}{A_{bt}} = 0.66 MPa.$$

- punching resistance verification:

$$\sigma_{uts,m} > \frac{N_{xy}\phi}{\pi d_0 t} = 16.89 \cdot 10^{-3} MPa.$$

Section D

The loads applied on section D are the following:

- axial load $N_D = 233.01N$;
- bending moment $M_{xD} = 0N \cdot m$;
- bending moment $M_{yD} = 8.11N \cdot m$;
- torque $M_{zD} = -0.59N \cdot m$.

In correspondence of section D, there is a pivot joint chosen from the Parker IPS catalogue [parker-ds], reported in figure 14.

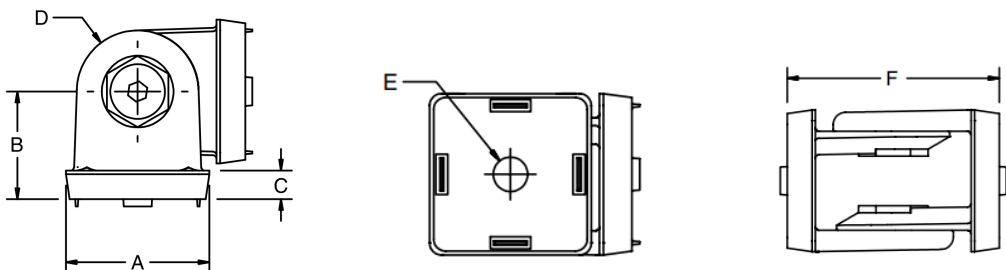


Figure 14: pivot joint, code 23-010, from the IPS catalogue [parker-ds]. In the drawing:
 $A = 40mm$, $B = 30mm$, $C = 9mm$, $D = 40mm$, $E = 8.5mm$, $F = 60mm$.

The loads action on section D are reported in figure 15

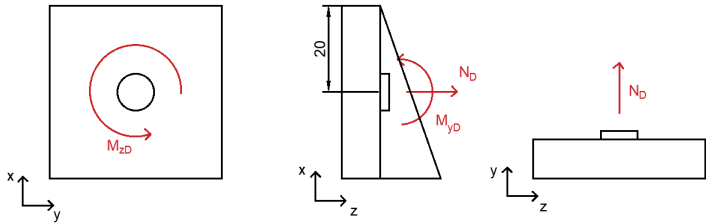


Figure 15: loads acting on section D

In this case, the sliding actions are given by the torque M_{zD} , figure 14(b). However, since there is a single screw positioned in the center of the section, they do not cause any shear on the screw.

Separating actions are given by the axial load and the bending moments. Assuming that the members are rigid it is possible to calculate the effects of the separating actions in both xz and yz planes. The load caused by the separating action, acting on the screw can be calculated as:

$$N_i = \frac{M_b h_i}{\sum_{i=1}^{n_b} h_i^2} + \frac{N}{n_b}$$

where h_i is the distance of the i -th bolt from the pivot point.

$$N_{xz} = \frac{M_{yD}}{h} + N_D = 638.33N$$

Considering the xz plane and assuming the pivot on the edge of the section, h is equal to $\frac{A}{2} = 20mm$. The tension resistance and punching verification can be performed as follow:

- tension resistance verification:

$$N_{xz} < \frac{\sigma_{uts} A_{bt}}{\phi}$$

Where σ_{uts} corresponds to the screw's ultimate tensile strength, A_{bt} to the bolt tensile cross-section and ϕ is the safety factor which, according to Eurocode3, is equal to $\frac{1.25}{0.9}$. As a consequence, it follows that:

$$\sigma_{uts} > \frac{N_{xz}\phi}{A_{bt}} = 24.22MPa$$

- punching resistance verification:

$$N_{xz} < \frac{\pi d_0 t \sigma_{uts,m}}{\phi}$$

Where $\sigma_{uts,m}$ corresponds to the member's ultimate tensile strength, d_0 the bolt head diameter and ϕ is the safety factor which, according to Eurocode3, is equal to $\frac{1.25}{0.6}$. Finally, t corresponds to the member's thickness, which can be calculated as the sum of the pivot joint thickness, $C = 9mm$, and the member's cross section, equal to $40mm$:

$$\sigma_{uts,m} > \frac{N_{xz}\phi}{\pi d_0 t} = 0.62MPa$$

Considering instead the xz plane we have:

$$N_{yz} = \frac{M_{xD}}{h} + N_D = 233.01N$$

thus:

- tension resistance verification:

$$N_{yz} < \frac{\sigma_{uts} A_{bt}}{\phi} \quad \Rightarrow \quad \sigma_{uts} > \frac{N_{yz}\phi}{A_{bt}} = 8.84MPa$$

- punching resistance verification

$$N_{yz} < \frac{\pi d_0 t \sigma_{uts,m}}{\phi} \quad \Rightarrow \quad \sigma_{uts,m} > \frac{N_{yz}\phi}{\pi d_0 t} = 0.23MPa$$

In conclusion, the bolt ultimate strength must be greater than $24.22MPa$, a value that allows to choose any bolt property class. In order to minimize the costs, property 4.6 is chosen.

Moreover, the verifications for crushing and punching provide the minimum member ultimate strength, $\sigma_{uts,m} > 0.23MPa$, value much smaller than the chosen member's UTS.

Note that for the verifications of the separating actions the rigid member approach was used, which is usually more conservative than the others. However, since the values obtained are far distant from the one of the selected materials, there is no need of a more precise verification.

As for most applications, the preload used to tighten the bolts is chosen to be 80% of the yield strength. At this point, the stiffness joint verification should be performed. However, due to the low external loads acting on the bolts, no issue will arise and there is no need to carry out this analysis.

4.4 Design and static verification of rack and gear

The verification continued with the parts responsible for actuating the machine, rack that is positioned on both tracks and gear attached on the motors' shaft. We focused on two important aspects, interference and tooth root bending resistance.

Interference condition

It's fundamental to check if this condition is fulfilled, because otherwise we could have a problem of undercut, when the tip of the rack cutter is moved beyond the base circle of the gear and the result is the weakening of the gear's teeth.

Interference condition is function of the minimum number of teeth of the pinion, in accordance with the following equation:

$$z_{min} = \frac{2}{\sin^2 \alpha}, \quad (1)$$

where α is the pressure angle, as we can see in figure 16. In our case we designed the profile with a pressure $\alpha = 20^\circ$, thus we have:

$$z_{min} = 17,$$

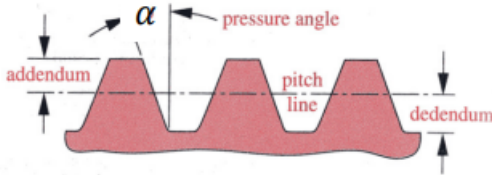


Figure 16: standard rack and pressure angle α .

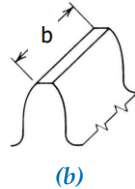
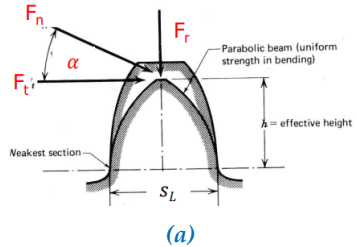


Figure 17: tooth details: section (a) and face width (b).

Gear design and verification

The gear attached to the motor's shaft is designed choosing as number of tooth $z = 18$; assuming that the motors actuating the machines can generate a power $P = 10W$ at $n = 50\text{rpm}$, the associated maximum generated torque is $T = 1.9\text{N} \cdot \text{m}$. Choosing as module m of the gear the value 2mm , then the nominal diameter of the gear is $d = zm = 36\text{mm}$ and the maximum force that can be transmitted by the gear is

$$F = \frac{T}{r} = 2 \frac{T}{d} = 106\text{N}$$

Tooth root fatigue resistance One of the most important problem in the usage of gears is the teeth fatigue resistance, due to the fact they're subjected to pulsating loads. In our analysis we used the Lewis method that consider the tooth as a cantilever beam and shear and compressive normal stresses are neglected.

According to such theory, the stress state acting on the tooth is

$$\sigma = \frac{F}{mbY_l}$$

where b is the face width (figure 17) and Y_l is the Lewis factor taking into account for the shape of the tooth; such parameter depends on both the number of teeth z and the pressure angle α , and for the given data it evaluates to $Y_l = 0.308$.

Given the ultimate tensile strength $\sigma_{uts} = 40\text{MPa}$ of plastic materials used in 3D printing machine and choosing a safety factor $\phi = 2$, reversing the Lewis equation gives us the minimum face width:

$$\sigma \leq \frac{\sigma_{uts}}{\phi} \quad \Rightarrow \quad b \geq \frac{F\phi}{Y_l m \sigma_{uts}} = 8.61\text{mm}$$

thus a width $b = 10\text{mm}$ for the teeth has been chosen.

Crushing verification The gear is mounted to the motors shaft by means of a $3 \times 3\text{mm}$ parallel key; the shaft is made of steel with high mechanical properties, while the gear,

that can be 3D-printed, has lower stress capability, thus we need to verify the member at crushing.

By the geometry of the gear reported in the annexes, the contact surface that is used to exchange the load is a rectangular surface of dimensions $b \times h = 10mm \times 1.292mm$; given the augmented force $F = 447N$ (as the radius where the force is applied is reduced to $r = 4.25mm$) that has to be exchanged, the mean pressure at the contact surface is

$$p = \frac{F}{bh} = 34.62MPa$$

Considering the allowable pressure $p_{all} = \sigma_{uts} = 40MPa$, then the safety factor against crushing of the gear is $\phi = 1.15$.

Gear and rack design With this calculation performed, using built-in tools provided by the software and simple sketches a custom design for both gear and rack has been developed in order to be 3D printed by the end user. Annex B.1 (page 26) reports the technical drawing of both parts.

Moreover exploiting the parametric capability of AutoDesk Inventor the rack length is fully modular and can be extended/reduced by a integer amount of teeth in order to match the 3D printer plate dimensions; in the drawing it has been considered a rack with $z = 60$ teeth giving an overall length $l = 377mm$.

5 Conclusions

The final robot is far from being finished, but this works provides a solid starting point to improve the actual machine design. At the current development state it has not been fully decided the final model of the motor used to actuate the system, however such decision will determine just a slight variation in the design of the plate used to connecting the motor to the plate of the linear guide; for this reason, the plate has not been reported in the technical drawings.

The designed assembly is also provided with a roller system running on the elevated track where the turret performing the operation can be built up on containing all the required tools.

For what concerns the actuation of the system, we assumed that the machine will be controlled in open loop using stepper motors; for this reasons at the end of all tracks a touch sensor need to be mounted in order to provide the control system (that will be an Arduino micro controller) with a reset point to rely on.

Such sensors can be positioned at one side of the ground tracks where a resting station should be designed, providing the turret a safe place to charge the battery placed on board of the turret and that guarantees protection from external actions.

Design improvements ideas The proposed design still leaves room for further improvement. One thing that might be improved is the kit shipping capability: as we can see in the final bill of materials (appendix A.2.1, page 25) we have 3 main big components with a length greater then $3m$, making their transportation and handling difficult. One way to improve the design is by studying proper axial connections in order to join beams with smaller lengths while still not impacting the design of the gear-rack coupling and leaving proper clearances for the roller linear guides.

A Appendix

A.1 Materials

Table A.1.1: list of available aluminium alloys for T slot profiles with relative mechanical properties (based on ASTM B-221 standard) and extruded profile vendor that provides this results.

ASTM code	σ_{uts} [MPa]	σ_{ys} [MPa]	E[GPa]	$\nu[\cdot]$	usage	vendors
6005-T5	262	241	70	0.33	profiles	Parker
6105-T5	262	241	70	0.33	profiles	80/20, Parker
6061-T6	262	241	70	0.33	accessories	Parker
6063-T6	206	172	70	0.32	profiles, accessories	Parker
6065-T6	206	172	68	0.32	profiles	tslots

Parameters of the table: σ_{uts} ultimate tensile strength, σ_{ys} yielding strength, E Young's module, ν Poisson's ratio.
 σ_{uts} and σ_{ys} are taken directly from the ASTM B-221-05 [ASTMB221] standard while other parameters came from T-slot producer's data-sheets [tslot-ds] [parker-ds] [8020-ds].

A.2 Bill of Materials

Table A.2.1: bill of material.

Code	Product	Quantity
	IPS Parker	
10-540	40mm light T-slot profile	1 × 700mm
10-540	40mm light T-slot profile	1 × 560mm
10-040	40mm T-slot profile	1 × 3 000mm
10-340	40mm tri-slot profile	2 × 4 000mm
10-081 ¹	16×80mm profile	3 × 300mm
20-102	machined gusset	3
23-010	pivot join	2
30-401	linear shaft roller components	12
13-505	"	1 × 3 000mm
13-106	"	1 × 3 000mm
13-505	"	2 × 4 000mm
13-106	"	2 × 4 000mm
20-058	M8 T-nut	14
20-049	M8 double T-nut	33 ³
20-050	M8 double T-nut	15
24-116-8	M8 × 1.25 button head screw, length 16mm	14
24-118-8	M8 × 1.25 button head screw, length 18mm	12
24-120-8	M8 × 1.25 button head screw, length 20mm	2
24-130-8	M8 × 1.25 button head screw, length 30mm	4
24-212-8	M8 × 1.25 flat head screw, length 12mm	4
24-320-4	M4 × 0.8 socket head screw, length 20mm	61 ³
24-330-8	M8 × 1.25 socket head screw, length 30mm	16
24-708	M8 spring washer	28
24-708	M8 spring washer	28
	Undefined manufacturer	
AS 1474 - M4 ²	Hexagonal nut	12
ISO 1580 M4x12 ²	Button head screw	12
	M8 × 1.25 male to M4 × 0.7 female thread reducer	54 ³
	3D printed parts	
Gear		3 ³
Rack		28 ³

¹: the piece need requires need to be machined in order to create the holes for inserting the socket head screws.

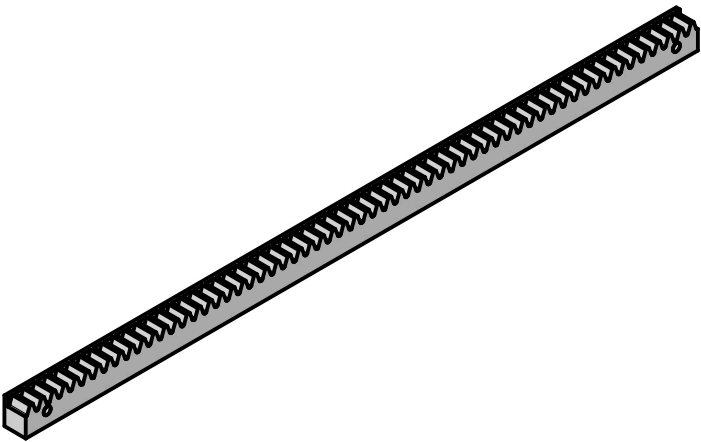
²: this component might change depending on the final motor chosen to drive the system.

³: the number might change depending on the size of the 3D printed rack; in this case it has been considered a component with z = 60 teeth, equivalent to a 377mm nominal length.

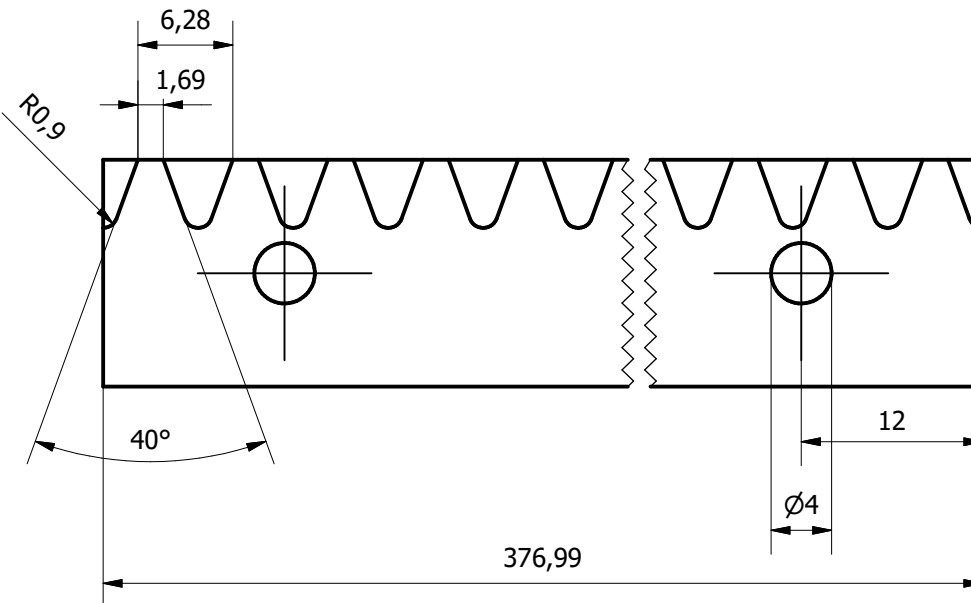
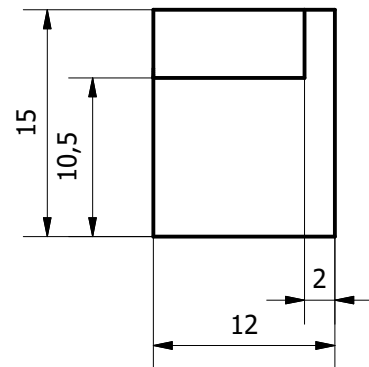
B Technical drawings

B.1 Gear and rack design

In the following page the detailed representation of the custom created rack and gear design is reported.



Rack profile created considering an involute profile design with modulus $m = 2mm$.



Designed by
Bontempelli Elia, Dalle Vedove Matteo, Rizzardi Alessandro, Zambotti Beatrice

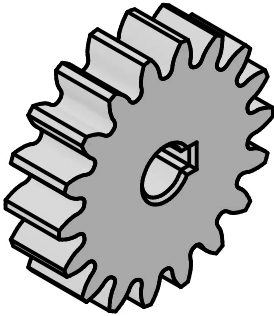
Date
26/08/2022

Università degli Studi di Trento
Department of Industrial Engineering

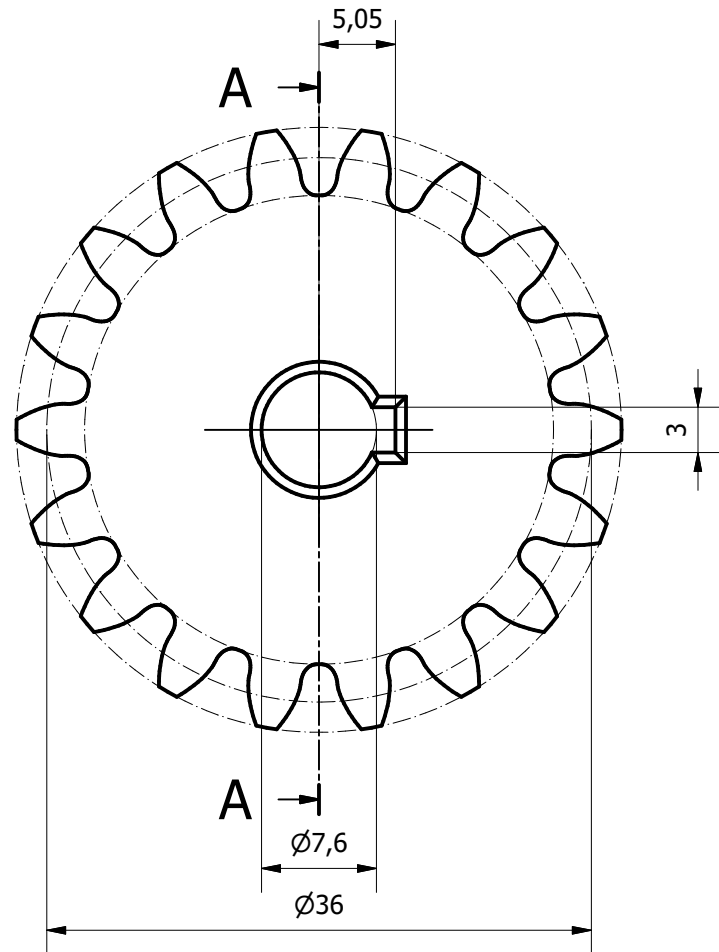
Rack Drawing

Mechanical Design for Mechatronics - Project

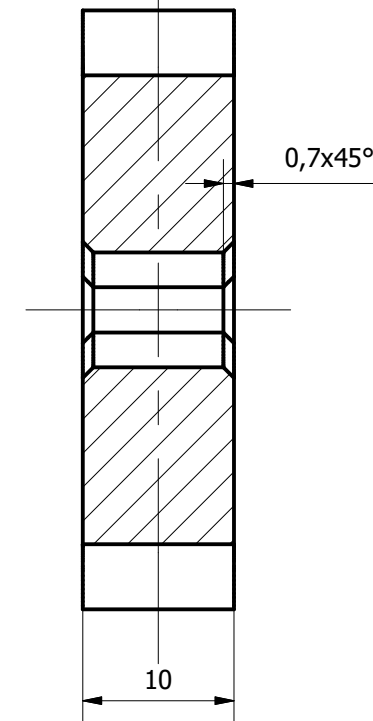
Sheet
1 / 1



Gear with $z = 18$ involute profiles teeth, modulus $m = 2\text{mm}$.
Reploted drawing is in scale 2:1



A-A (2 : 1)



Designed by
Bontempelli Elia, Dalle Vedove Matteo, Rizzardi Alessandro, Zambotti Beatrice

Date
26/08/2022

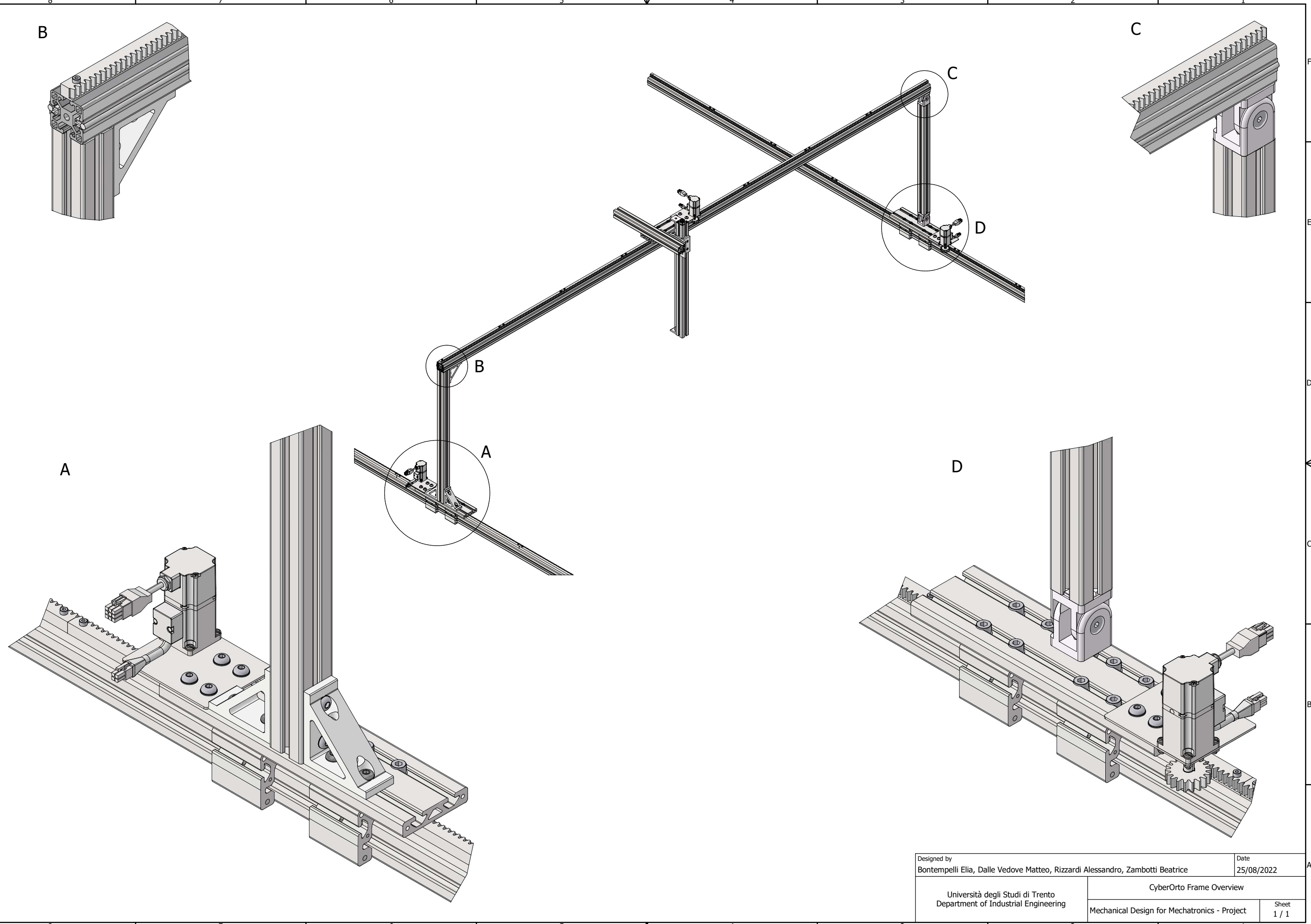
Università degli Studi di Trento
Department of Industrial Engineering

Gear Drawing

Mechanical Design for Mechatronics - Project

Sheet
1 / 1

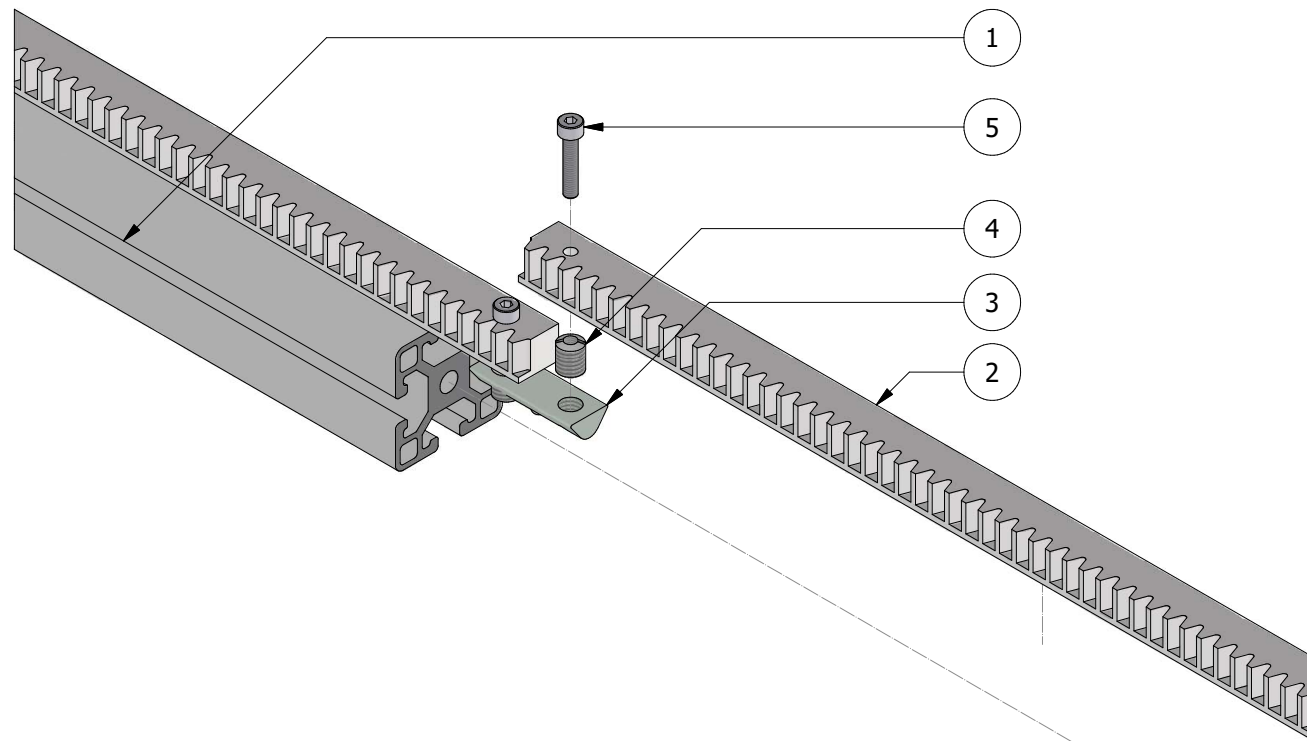
B.2 Final CAD



Designed by Bontempelli Elia, Dalle Vedove Matteo, Rizzardi Alessandro, Zambotti Beatrice	Date 25/08/2022
Università degli Studi di Trento Department of Industrial Engineering	CyberOrto Frame Overview
Mechanical Design for Mechatronics - Project	Sheet 1 / 1

B.3 Connection assembly details

In the following pages it's possible to find instructions on how to assembly the rack on top of the T-slot profiles and how to assemble the main junctions of the frame, namely connections *A*, *B*, *C* and *D*.



ELENCO PARTI

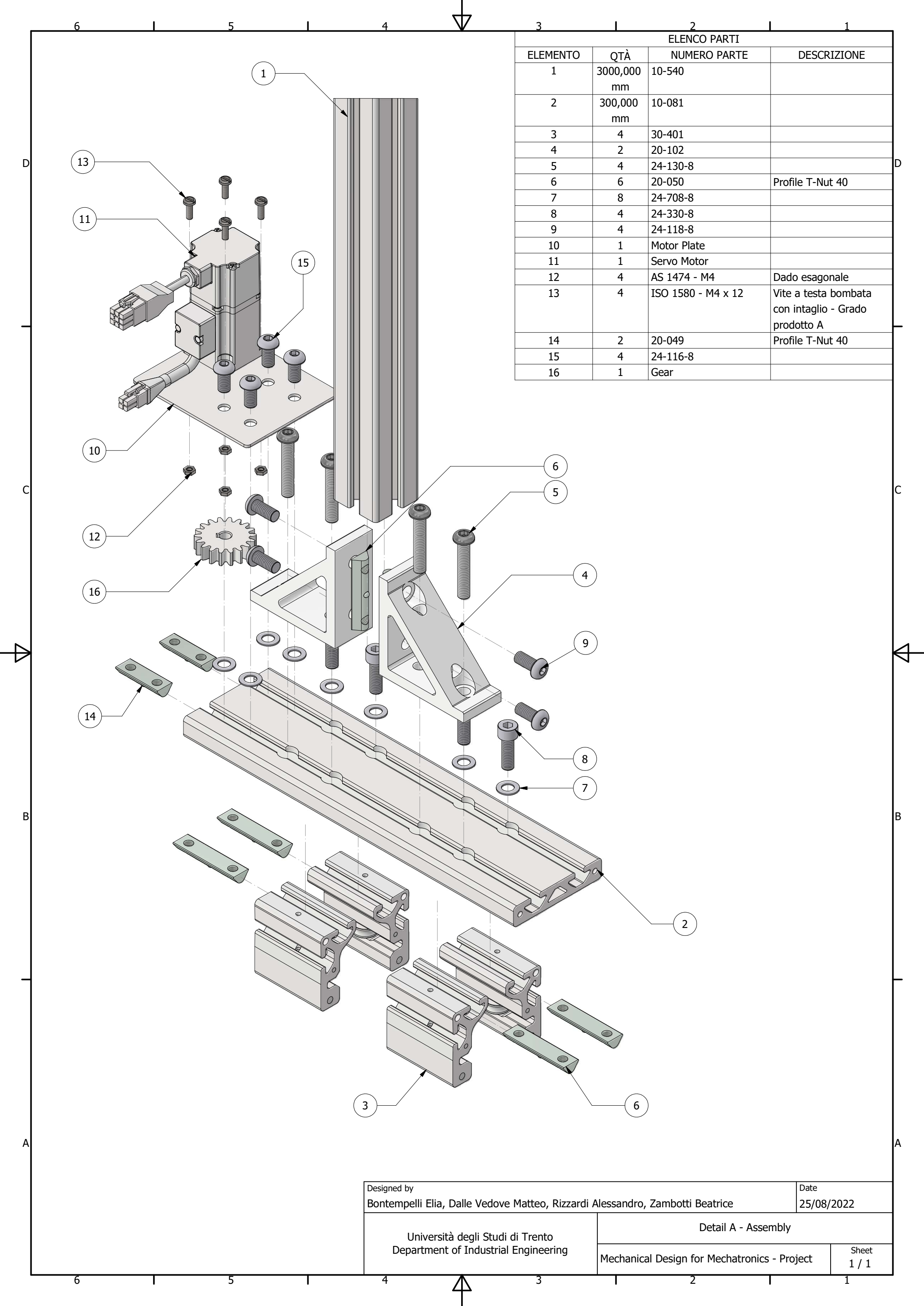
ELEMENTO	QTÀ	NUMERO PARTE	DESCRIZIONE
1	3000,000 mm	10-040	
2	3	Rack	
3	2	20-049	Profile T-Nut 40
4	4	Thread reducer	M8x1.25 male to M4x0.7 female
5	6	24-320-4	M4x0.7 Socket Head screw
6	2	20-051	Profile T-Nut 40

Designed by
Bontempelli Elia, Dalle Vedove Matteo, Rizzardi Alessandro, Zambotti Beatrice

Date
24/08/2022

ELENCO PARTI

ELEMENTO	QTÀ	NUMERO PARTE	DESCRIZIONE
1	3000,000 mm	10-540	
2	300,000 mm	10-081	
3	4	30-401	
4	2	20-102	
5	4	24-130-8	
6	6	20-050	Profile T-Nut 40
7	8	24-708-8	
8	4	24-330-8	
9	4	24-118-8	
10	1	Motor Plate	
11	1	Servo Motor	
12	4	AS 1474 - M4	Dado esagonale
13	4	ISO 1580 - M4 x 12	Vite a testa bombata con intaglio - Grado prodotto A
14	2	20-049	Profile T-Nut 40
15	4	24-116-8	
16	1	Gear	



Designed by
Bontempelli Elia, Dalle Vedove Matteo, Rizzardi Alessandro, Zambotti Beatrice

Date
25/08/2022

Università degli Studi di Trento
Department of Industrial Engineering

Detail A - Assembly

Mechanical Design for Mechatronics - Project

Sheet
1 / 1

6 5 4 3 2 1

ELENCO PARTI

ELEMENTO	QTÀ	NUMERO PARTE	DESCRIZIONE
1	1	20-102	
2	2	20-050	Profile T-Nut 40
3	4	24-118-8	
4	3000,000 mm	10-540	
5	3000,000 mm	10-040	

D

D

C

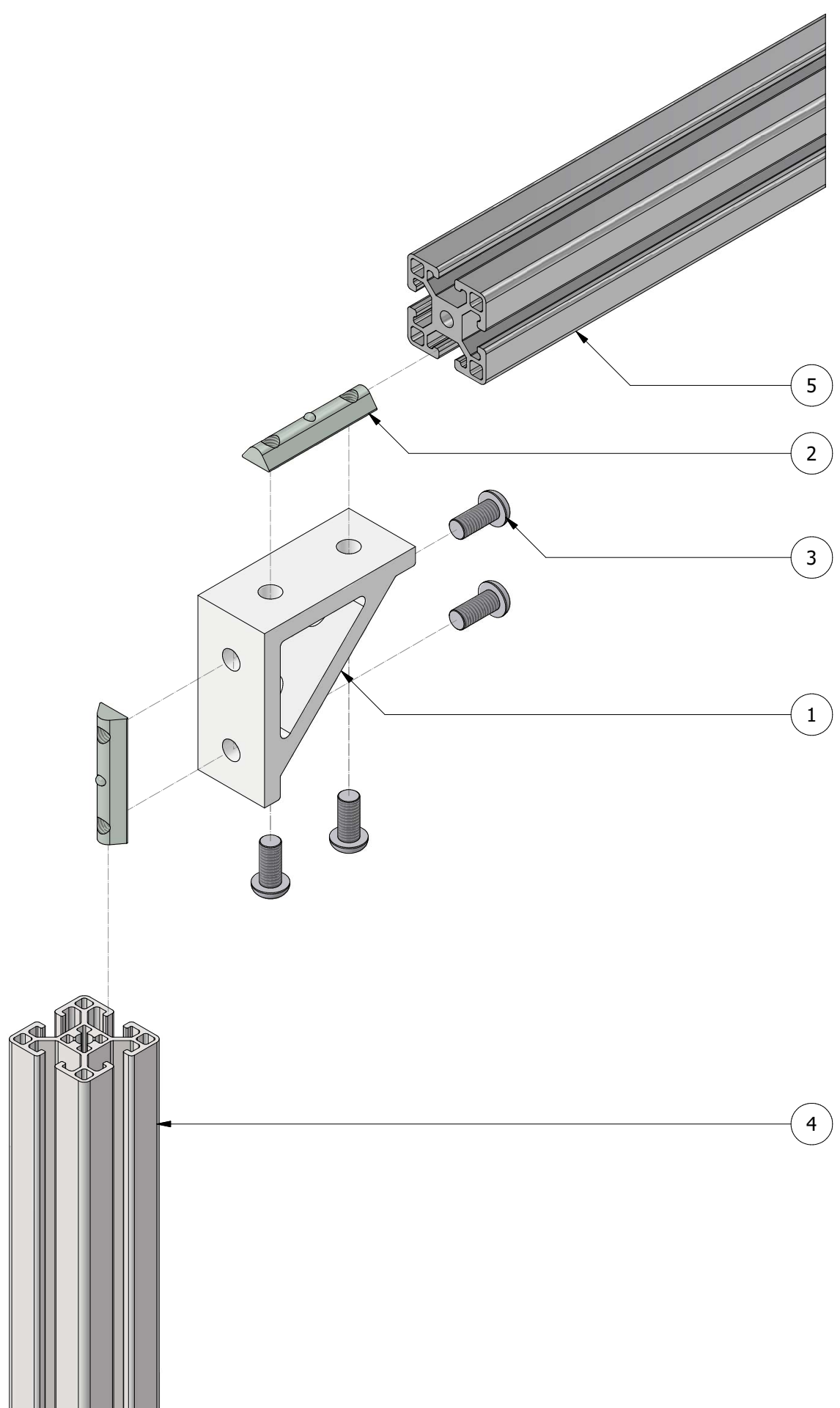
C

A

A

B

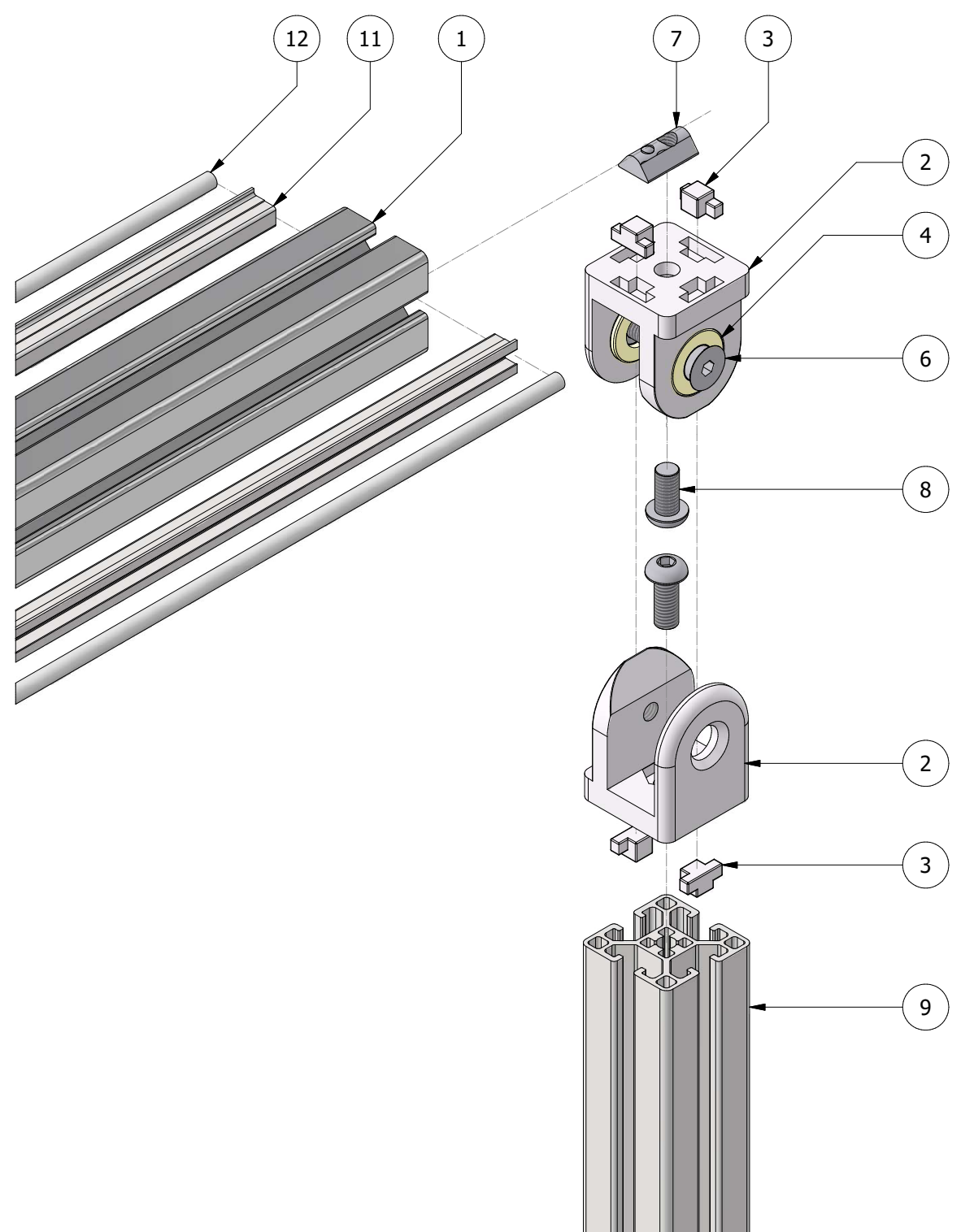
B



6 5 4 3 2 1

Designed by Bontempelli Elia, Dalle Vedove Matteo, Rizzardi Alessandro, Zambotti Beatrice	Date 24/08/2022
Università degli Studi di Trento Department of Industrial Engineering	Detail B - Assembly
Mechanical Design for Mechatronics - Project	Sheet 1 / 1

ELENCO PARTI			
ELEMENTO	QTÀ	NUMERO PARTE	DESCRIZIONE
1	3000,000 mm	10-040	
2	2	23-010Z1	
3	4	23-010Z2	
4	2	23-010Z3	
5	2	23-010Z4	
6	2	24-212-8	
7	1	20-058	
8	1	24-116-8	
9	100,000 mm	10-540	
10	1	24-120-8	
11	200,000 mm	13-106	
12	200,000 mm	13-513	

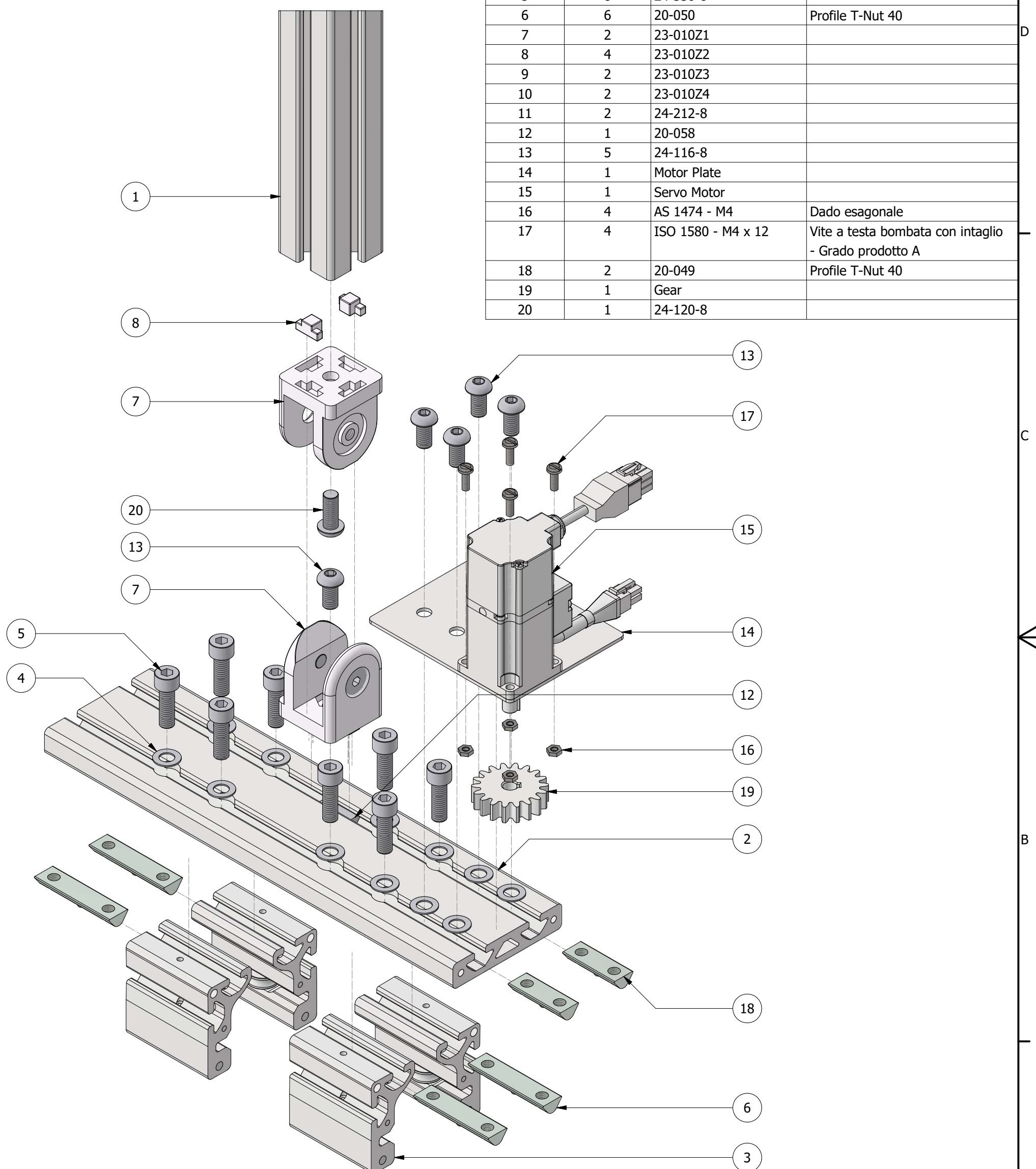


Designed by Bontempelli Elia, Dalle Vedove Matteo, Rizzardi Alessandro, Zambotti Beatrice	Date 24/08/2022
Università degli Studi di Trento Department of Industrial Engineering	Detail C - Assembly
Mechanical Design for Mechatronics - Project	Sheet 1 / 1

6 5 4 3 2 1

ELENCO PARTI

ELEMENTO	QTÀ	NUMERO PARTE	DESCRIZIONE
1	100,000 mm	10-540	
2	300,000 mm	10-081	
3	4	30-401	
4	12	24-708-8	
5	8	24-330-8	
6	6	20-050	Profile T-Nut 40
7	2	23-010Z1	
8	4	23-010Z2	
9	2	23-010Z3	
10	2	23-010Z4	
11	2	24-212-8	
12	1	20-058	
13	5	24-116-8	
14	1	Motor Plate	
15	1	Servo Motor	
16	4	AS 1474 - M4	Dado esagonale
17	4	ISO 1580 - M4 x 12	Vite a testa bombata con intaglio - Grado prodotto A
18	2	20-049	Profile T-Nut 40
19	1	Gear	
20	1	24-120-8	



Designed by
Bontempelli Elia, Dalle Vedove Matteo, Rizzardi Alessandro, Zambotti Beatrice

Date
24/08/2022

Università degli Studi di Trento
Department of Industrial Engineering

Detail D - Assembly

Mechanical Design for Mechatronics - Project

Sheet
1 / 1

6 5 4 3 2 1

C Bibliography and references

In order of first appearance: